Supporting Material

Mapping the Importance of Four Factors in Creating Monovalent Ion

Michael Thomas, Dylan Jayatilaka, and Ben Corry

Mapping the Importance of Four Factors in Creating Monovalent Ion Selectivity in Biological Molecules: Supplementary Material

Michael Thomas, Dylan Jayatilaka and Ben Corry

Detailed Simulation Parameters used for Model Systems

Periodic boundary conditions were employed for all bulk systems under an NPT ensemble (except for the bulk abstract ligand systems described earlier) at 1 atmosphere and 310K, (using langevin dynamics) and 1 fs timestep. A cut off distance of 12 Å is used for electrostatic and van der Waals interactions in non-periodic systems. In periodic systems, particle mesh Ewald summation was used to calculate electrostatic interactions unless stated otherwise.

λ windows for thermal fluctuation models FEPs

Although in hindsight it turned out to be unnecessary as the simulations converged well, these FEP simulations were conducted using 34 λ windows, with λ values of 0, then 10^n for $n = -7, -6 \ldots, -2$ then 0.05 then incrementing by 0.05 to $\lambda = 0.95$, then $1 - 10^n$ for $n =, -2, -3, \ldots, -7$ then 1.

Error estimation

Uncertainties in the free energies of the model systems were estimated by obtaining the standard error of 8 replicate FEP simulations (4 forward and 4 reverse morphs) for the situations in which $q = 0.5$, $n = 1, 5, 8$ and $k = 0$. The standard errors in the mean were all below 0.005 kcal/mol.

Verifying Simulation Results

Force Field. The results in this study may be dependent on the choice of force field as well as the environment surrounding the model systems. To study the influence of the choice of force field on the results, the OPLS force field (1) was used to reproduce the selectivity map in Fig. 3 A of the main text. The group I ion parameters (2) and the carbon-oxygen bonding and non-bonded parameters for the model ligands used OPLS, while angle and dihedral parameters for the model ligands were taken from the CHARMM parameter set, as they were not available in OPLS. The OPLS selectivity map, seen in Fig. 5 A, maintains the characteristic shape of the original figure. The difference in ΔG values between the two ranges is plotted in figure 5 C and is between 3 kcal/mol at the extremes, with the majority of useful energies (those that would not fall in the exclusion zone) being less than 2 kcal/mol. The difference in ΔG between CHARMM and OPLS found for the specific molecules studied in the main text is less than 1 kcal/mol.

Simulation Setup. The nature of the medium surrounding the model system may influence the free energy values. Three different model systems were simulated to quantify this effect. Each consists of n model ligands constrained so that the oxygen atoms are in a spherical shell of 3.5 Å (4.0 Å for Cs$^+$). Enveloping this was (i) vacuum, (ii) a spherical shell of model ligands, 10.5 Å in radius and (iii) a 30×30×30 Å periodic box of model ligands, which for simplicity will be referred to as the 'sphere', 'sphere in a sphere' and 'sphere in a box' models. The additional model ligands have the same partial charges on the carbon and oxygen atoms as those within the inner sphere. Systems (i) and (ii) were simulated using $n = 1 - 10, q = 0.1 - 1$ while (iii) only using (n,q)=(8,0.5) due to the large computational time involved. A comparison of the three systems using (n,q)=(8,0.5) is summarised in table 3 (a comparison for all (n,q) between systems (i) and (ii) is made graphically in Fig. 5 B and D). While there are significant differences in the total predicted selectivity of the model binding site shown in table 3, each is still a reasonable reflection of the experimental selectivity value of 5-6 kcal/mol seen in KcsA (3–6) that has a binding site of similar composition to the model. The percentage contributions to selectivity by coordination number restriction, χ_n, and dipole moment, χ_q differ at most by 7%, which is quite remarkable as it implies that the relative makeup of the total selectivity varies little regardless of the total selectivity.

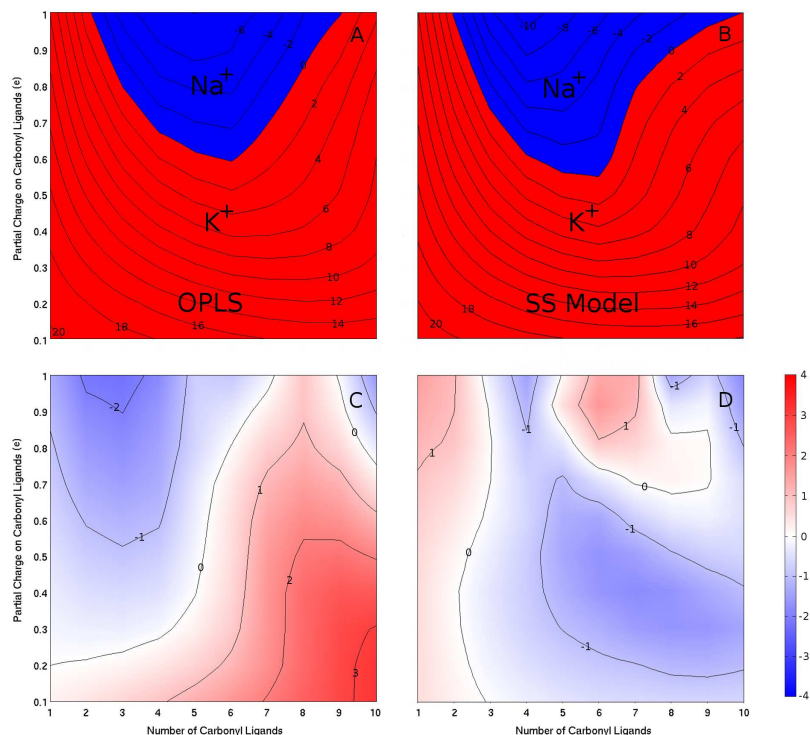The point of these additional simulations was to see how the effect of the

Figure 5: (A) Selectivity map using OPLS force field. (B) Selectivity map using 'sphere in a sphere' (SS) model system. (C) Difference between CHARMM and OPLS selectivity maps. (D) Difference between selectivity maps produced using sphere and SS model systems. All energies in kcal/mol. Red depicts K^+ selectivity, blue depicts Na^+ selectivity. Colours in (C) and (D) are used for clarity.

surrounding medium influences the selectivity of the model binding sites. As each binding site will have a different environment it is difficult to be sure which of our test calculations best mimics the specific site. These studies do, however, give an indication of the range of uncertainty in our predictions that is created by the details of the medium surrounding each site. The 10.5 Å sphere of bulk model ligands in our sphere in a sphere system allows for rapid energy calculations as required for constructing selectivity maps across a wide range of parameters. To test how similar the results of this case are

3

System	Force Field	ΔG_W	ΔG_{nq}	ΔG_n	ΔG_q	χ_n	χ_q
S	CHARMM	21.06	6.58	N/A	N/A	N/A	N/A
S	OPLS	21.68	5.07	N/A	N/A	N/A	N/A
SS	CHARMM	21.06	5.53	2.16	3.37	60.9%	39.1%
SS	OPLS	21.68	2.82	0.96	1.86	66.0%	34.0%
SB	CHARMM	21.06	8.56	3.02	5.54	64.7%	35.3%
SB	OPLS	21.68	4.50	1.86	2.64	58.7%	41.4%

Table 3: Summary of model systems and associated ΔG and χ_n and χ_q values for (n,q)=(8,0.5). S, SS and SB signify sphere, sphere in a sphere and sphere in a box model systems respectively. ΔG_W is the free energy of morphing Na^+ to K^+ in a 30×30×30 Å period box of TIP3P water. ΔG_{nq} is the total selectivity of the model system. Other ΔG values are described in the methods section of the main text. All energies are in kcal/mol

to those in a larger bulk medium we examined how ΔG_{nq} depends on the size of the bulk sphere for the (n,q)=(8.0.5) sphere in a sphere model system. As shown in table 4 the small sphere gives fairly similar results to those in a larger, more bulk like medium.

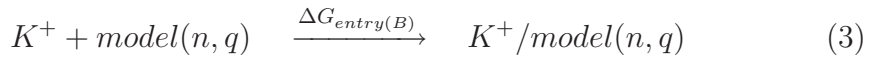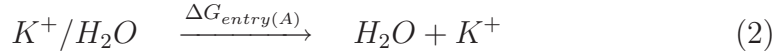| Sphere size	ΔG_{nq}
Vacuum	6.58
10.5 Å	5.53
15 Å	5.87
20 Å	5.85
25 Å	5.92
30 Å	5.93

Table 4: ΔG_{nq} (kcal/mol) for Na^+ and K^+ in a sphere in a sphere model system with (n,q)=(8.0.5) for models with differing radii of the outer model ligand containing sphere.
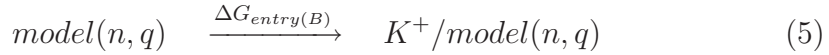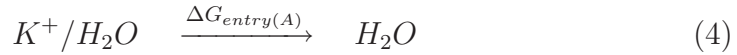
Correction Terms for ΔG_{entry}

ΔG_{entry} is the free energy of moving an ion from bulk water into a model site.

$$K^+/H_2O + model(n, q) \quad \xrightarrow{\Delta G_{entry}} \quad H_2O + K^+/model(n, q) \qquad (1)$$
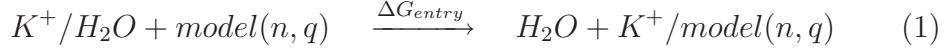
This is constructed from two separate binding free energies:

$$K^+/H_2O \quad \xrightarrow{\Delta G_{entry(A)}} \quad H_2O + K^+ \qquad (2)$$

$$K^+ + model(n, q) \quad \xrightarrow{\Delta G_{entry(B)}} \quad K^+/model(n, q) \qquad (3)$$

Normally the double-annihilation method is used to calculate the binding free energy (7). However, since K^+ cancels out when equations 2 and 3 are combined, we can reduce the calculation to two FEP calculations:

$$K^+/H_2O \quad \xrightarrow{\Delta G_{entry(A)}} \quad H_2O \qquad (4)$$

$$model(n, q) \quad \xrightarrow{\Delta G_{entry(B)}} \quad K^+/model(n, q) \qquad (5)$$

The corrections terms that are needed to yield the binding free energies by using the double annihilation method, as described by Gilson et al (8), cancel out.

Additional corrections must be applied when calculating free energies of introducing a charged species into an explicit solvent systems, which in this case is equation 4. These corrections terms are described in detail by Kastenholz and Hünenburger (9). Two of the corrections discussed are applicable to this situation; approximations in the electrostatic interactions introduced from using cut off truncation (type A correction), and artificial polarisation of the solvent molecules from using a periodic boundary condition (type B correction). The corresponding correction terms are ΔG_A^{CT} and ΔG_B^{CT} (where CT means cut off truncation method). ΔG_A^{CT} is further divided into two parts; a correction for electrostatic interactions outside the cut off sphere, ΔG_{A1}^{CT}, and a inside the cutoff sphere, ΔG_{A2}^{CT}, so that

$$\Delta G_A^{CT} = \Delta G_{A1}^{CT} + \Delta G_{A2}^{CT} \qquad (6)$$

ΔG_{A1}^{CT} and ΔG_B^{CT} are trivial to calculate if ΔG_A^{CT} is known.

$$\Delta G_{A1}^{CT} = -(8\pi\epsilon_0)^{-1} q_I^2 (1 - \epsilon_S^{-1}) R_C^{-1} \qquad (7)$$

$$\Delta G_{\mathrm{B}}^{\mathrm{CT}} = -\frac{R_I}{R_C} 10^{\mu[L/(2R_C)]+\nu}[(8\pi\epsilon_0)^{-1}q_I^2(1-\epsilon_S^{-1})R_I^{-1} + \Delta G_{\mathrm{A}}^{\mathrm{CT}}] \qquad (8)$$

where ϵ_0 is the permittivity of vacuum, q_I the ionic charge, $\epsilon_S = 78$ the permittivity of the solvent, $R_C = 12$ Å the cut off radius, $R_I = 1.33$ Å the ionic radius, $L = 30$ Å is the edge length of the solvent box and $\mu = -2.20$ and $\nu = 1.29$ are constants. $\Delta G_{\mathrm{A2}}^{\mathrm{CT}}$ is then given by:

$$\Delta G_{\mathrm{A2}}^{\mathrm{CT}} = -(8\pi\epsilon_0)^{-1}q_I^2(1-\epsilon_S^{-1})\times[R_I^{-1}-R_C^{-1}+\sum_{k=-1}^{N_a}ka_kR_c^{-k-1}\int_{R_I}^{R_C}dr\ r^{k+1}p(r)]$$

$$(9)$$

We can define

$$C = R_C^{-1} + \sum_{k=-1}^{N_a}ka_kR_c^{-k-1}\int_{R_I}^{R_C}dr\ r^{k+1}p(r) \qquad (10)$$

where C is a constant. We can now determine the value of C is for the case explored by Kastenholz and Hünenburger (9), Na^+ in a periodic water box. We take $\Delta G_{\mathrm{A2}}^{\mathrm{CT}} = 17.61$ kJ/mol from table III. Assuming that this system and our K^+ periodic water box system is similar enough for C to be equal in both cases, we can now solve $\Delta G_{\mathrm{A2}}^{\mathrm{CT}}$ for the K^+ system:

$$\Delta G_{\mathrm{A2}}^{\mathrm{CT}} = -(8\pi\epsilon_0)^{-1}q_I^2(1 - \epsilon_S^{-1}) \times [R_I^{-1} - C] = 17.61\,\mathrm{kcal/mol} \qquad (11)$$

Now the binding free energy correction, ΔG_{corr}, is:

$$\Delta G_{\mathrm{corr}} = \Delta G_{\mathrm{A1}}^{\mathrm{CT}} + \Delta G_{\mathrm{A2}}^{\mathrm{CT}} + \Delta G_{\mathrm{B}}^{\mathrm{CT}} = -9.9\,\mathrm{kcal/mol} \qquad (12)$$

Ion Parameters

The vdW parameters we have used for Na^+ and K^+ are those developed and used by Roux et al in a number of recent works (13–15) (originating from the work of Beglov and Roux (16)). The values used for Rb^+ and Cs^+ also come from Roux et al while only those for Li^+ are developed here. The results we have presented for Rb^+, Cs^+ and Li^+ (eg in Fig 3B) are intentionally only qualitative given that the parameters for these ions have been less thoroughly tested. The vdW parameters used in this study are given in table 5 along with ion-water distances and coordination numbers (table 6) and compared to experimental values. We note that experimentally determining coordination numbers is particularly difficult for Cs^+ given its structural lability in water (17).

Ion	ϵ	$r_{min}/2$	First ion-oxygen RDF peak (Å)	exp. ion-oxygen distance (Å)
Li$^+$	-0.0030	1.137	1.87 ± 0.02	1.96 (10)
Na$^+$	-0.0469	1.36375	2.30 ± 0.05	2.39 - 2.42 (11)
K$^+$	-0.0870	1.76375	2.70 ± 0.05	2.7 - 2.9 (12)
Rb$^+$	-0.150	1.90	2.90 ± 0.05	2.80 - 3.05 (12)
Cs$^+$	-0.1900	2.100	3.15 ± 0.05	2.95 - 3.21 (12)

Table 5: Lennard-Jones parameters of the ions used in this study. Included are the distances in the first peak of the RDF in an 30x30x30 Å TIP3 water box and the experimental value of the ion-ligand distance. Error in the simulated value signifies the uncertainty in identifying this peak. Where multiple experiments have been conducted, a range of values is given.

Ion	This Study	Experimental	Molecular Dynamics	Quantum Methods
Li$^+$	4.0	3-6 (18), 3.0-6.5 (19)	4 (18), 4.1 (20)	4 (18)
Na$^+$	5.7	4-8 (18), 4.9 (19)	5-7 (18), 5.9 (20)	4-6 (18), 5.5(21)
K$^+$	7.0	4-8 (18), 6-8 (12), 5.3 (19)	6-8 (18), 7.2 (20)	4-8 (18), 6.2 & 6.8 (21)
Rb$^+$	7.8	5.6 (22), 6.4-7.4 (23), 6-8 (12), 6.5 (25), 6.9 (19)	7.8 (20), 8.5 (24)	7.1 (24)
Cs$^+$	9.6	8.2 (26), 3-9 (12), 8.1 (27), 7.9 (28)	9.6 (20)	7.8-9.1 (17)

Table 6: Coordination numbers of the ions used in this study determined in a periodic water box with Cl$^-$ counterion compared with published values derived from experiment, other molecular dynamic simulations and various quantum methods.

Heterogeneous Ligand Partial Charges

As noted in the article, the effects of having ligands with partial charges that deviate substantially from the average partial charge on all the ligands surrounding the ion is a source of disparity between predicted and simulated ΔG values. To investigate this issue we have constructed 8 additional maps involving combinations of two types of ligands. In these we have up to two TIP3 waters as ligands and/or up to two fully charged acidic residues (a

model ligand containing a +1.0 e charge on the carbon and a -1.0 e charge on the oxygen), while the remainder of the ligands making up the total coordination number n are ligands with controllable dipole moment as in the main text.

It is evident from Figs. 6 and 7 that as the number of ligands with unitary charge in a system increases (ie inclusion of acidic residues) the more selective the system becomes for the the smaller ions. Indeed the presence of 2 fully charged ligands makes it essentially impossible to select for K^+ via restricting coordination numbers, indicating the dominance of dipole moment effects on selectivity under such conditions. In contrast, an increase in the number of water molecules in the system dissipates selectivity; it reduces the degree of selectivity but does not appear to change which ion is selected given the nature of the remaining ligands.

These results are particularly interesting given recent discussion of the differences in selectivity between the KcsA channel and the non-selective NaK channel that have similar, but not identical selectivity filters. It has been suggested that the structure of the NaK channel allows for more water to contact ions in the binding sites which act to reduce the selectivity of these sites due to the differing dipole moment of water and carbonyl ligands (14). Our data is certainly consistent with this hypothesis. Even if the number of ligands coordinating an ion in an NaK binding site remains fixed at 8 or more as seen in KcsA, then Fig. 7 indicates that the substitution of two carbonyl groups with two water molecules reduces selectivity by more than 2 kcal/mol. Fowler et al have noted, however, that the coordination number of ions in NaK may be less constrained than in KcsA (29). This observation would provide an alternative route to reduce selectivity in NaK compared to KcsA. It is likely that both the presence of additional water around the ion and the greater freedom in determining coordination numbers in NaK compared to KcsA combine to reduce K^+ selectivity.

Sites where coordination numbers can change

All the model systems discussed so far have assumed that the coordination number remains constant as one ion type is exchanged with another. While this is reasonable in many cases, there are some in which the coordination number changes with ion type. If the coordination number changes between 'optimal' values for each ion type, i.e. there is no restriction on coordination
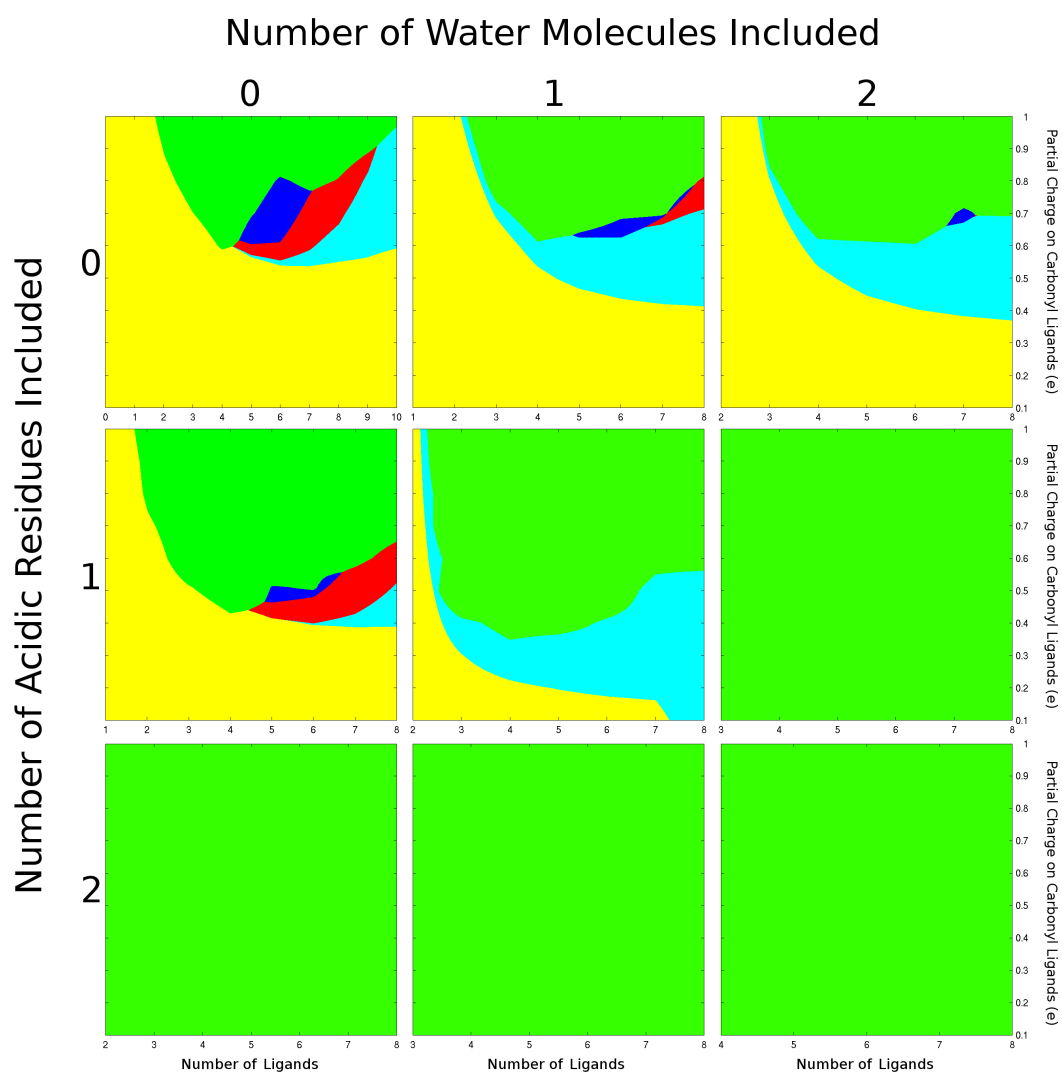
Figure 6: Selectivity maps of (n,q) model systems with water and/or acidic residues participating in ion coordination for group I ions with regions shown that are selective for Li$^+$ (green), Na$^+$ (blue), K$^+$ (red), Rb$^+$ (cyan) and Cs$^+$ (yellow). Exclusion zones have not been calculated for these maps.
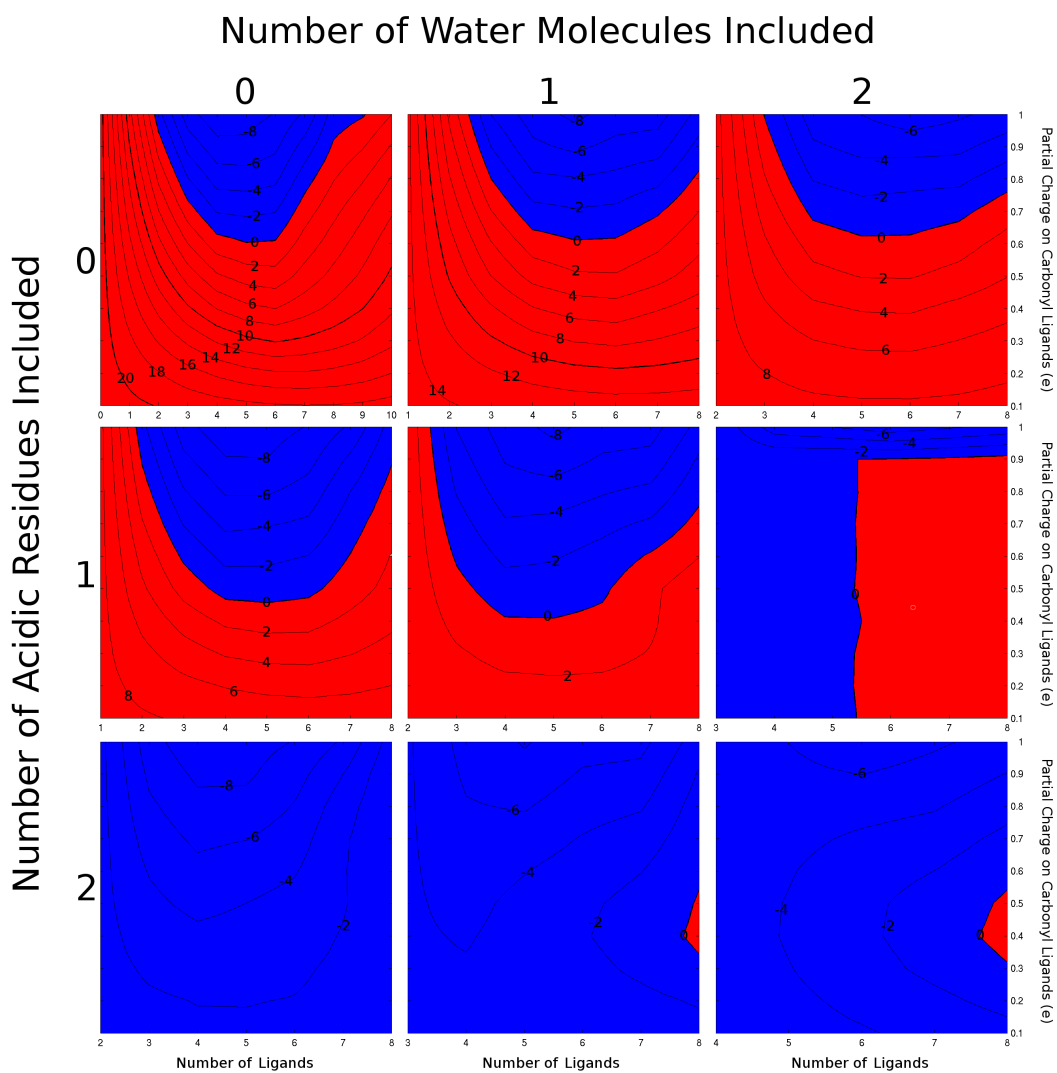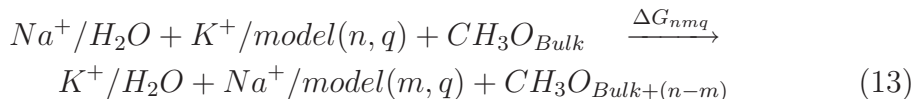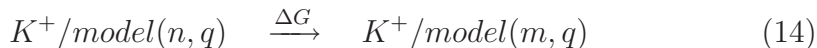
9

Figure 7: Selectivity maps of (n,q) model systems with water and/or acidic residues participating in ion coordination for K^+ and Na^+ shown with 2 kcal/mol contour differences in ΔG_{nq}. Regions that yield K^+ selectivity are indicated in red, Na^+ selectivity in blue. Exclusion zones have not been calculated for these maps.

number, then coordination number restriction cannot lead to selectivity. In this case selectivity can be accurately predicted using just a study of dipole moment contributions such as in Fig. 2 of the main text. However, it is also possible that the coordination number can alter with ion type, but not be able to obtain the ideal values, in which case coordination number restriction can still create ion selectivity without demanding that the number of coordinating ligands remain constant. These cases can be studied by examining the selectivity of a site that has n fold coordination for one ion type and m fold coordination for another. To create this, an ion exchange equation can be constructed using our model system in equation 2 in the main text, along with additional MD FEP simulations where a model ligand is removed gradually from the model system and added to bulk model ligand;

$$Na^+/H_2O + K^+/model(n,q) + CH_3O_{Bulk} \xrightarrow{\Delta G_{nmq}}$$
$$K^+/H_2O + Na^+/model(m,q) + CH_3O_{Bulk+(n-m)} \tag{13}$$

The additional MD FEP simulations are:

$$K^+/model(n,q) \xrightarrow{\Delta G} K^+/model(m,q) \tag{14}$$

and

$$CH_3O_{Bulk} \xrightarrow{\Delta G} CH_3O_{Bulk-1} \tag{15}$$

Fig. 8 shows the results for four different partial charges, allowing selectivity to be predicted in cases where the coordination number changes with ion type. Bostick et al (30) produced graphs using the same reaction but using water instead of model ligands that look very similar to our figure with $q = 0.5$. Our graphs extend their analysis to cover a range of different ligand types.

Restrained cavity size selectivity maps

Six systems were investigated with $r_{Na^+} = r_{K^+}$ and variable RMSD, with different ligand number and partial charge (n,q)= $(5, 0.5)$, $(5, 0.6)$, $(6, 0.5)$, $(6, 0.6)$, $(6, 0.7)$ and $(8, 0.5)$ (Fig. 9). In all six situations, it is observed that cavity size effects play an important role in ion selectivity when the ligands are held firmly in place. At low RMSD (> 0.5 Å) there is an increasingly
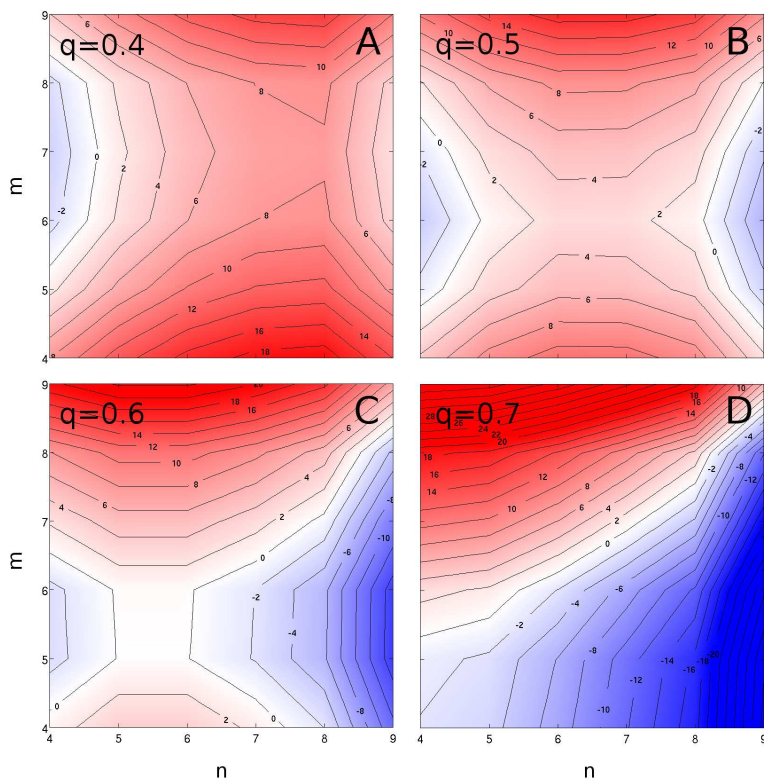
Figure 8: Free energies of selectivity between n ligands coordinating to K^+ and m ligands coordinating to Na^+ for partial charges of (A) 0.4, (B) 0.5, (C) 0.6 and (D) 0.7, according to equation 13. Regions of K^+ selectivity are shown in red, Na^+ in blue. Contours are spaced at 2 kcal/mol intervals.

significant contribution to Na^+ selectivity when $r < 2.5$ Å and to K^+ when $r > 2.5$ Å. However, when the flexibility of the ligands is larger such that they can move to accommodate differently sized ions (ie RMSD > 0.5 Å) the influence of cavity size diminishes. The total selectivity plateaus with increasing RMSD toward the corresponding ΔG value on the selectivity maps shown in Fig. 2B of the main text. As noted in the text we found that restrictions on the thermal fluctuations of coordinating ligands rather than restrictions on the cavity size itself appeared more important in the molecules
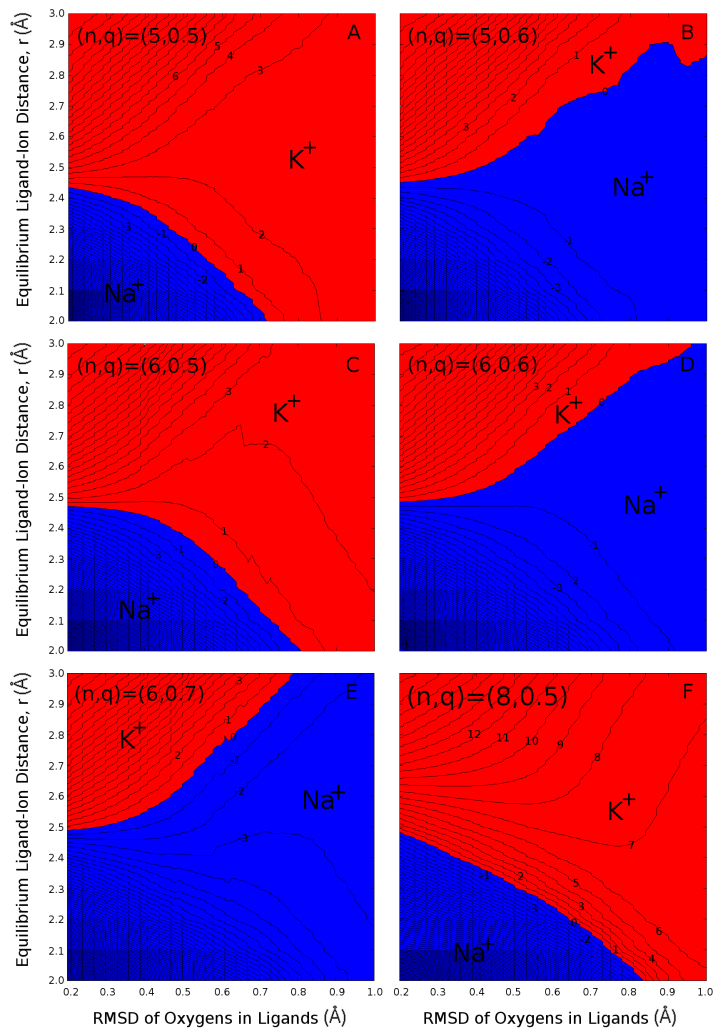
studied.

Figure 9: Influence of cavity size (as measured by the equilibrium ion-ligand distance r and RMSD) on ion selectivity for (n, q) systems (A)$(5, 0.5)$, (B)$(5, 0.6)$, (C)$(6, 0.5)$, (D)$(6, 0.6)$, (E)$(6, 0.7)$ and (F) $(8, 0.5)$. Red indicates preference for K^+ while blue indicates preference for Na^+. The interface between the two colours is 0 kcal/mol with each contour line representing 1 kcal/mol.

Additional thermal fluctuation maps

See Fig. 10.

Discussion of specific ion binding sites

As noted in the main text, we validated our predictive scheme by comparison with detailed MD simulations of a number of ion selective molecules. For simplicity, we concerned ourselves only with molecules showing selectivity between Na^+ and K^+. These included three ion channels KcsA (simulations described previously (31)), NaK and a simple model of a sodium channel selectivity filter; two amino acid transporters LeuT and Glt_{Ph}; a DNA quadruplex; the enzyme aminoimidazole riboside kinase; valinomycin, nonactin and 18-crown-6. Details of the parameters used in each simulation are given in table 7 and in the subsequent text. A more detailed discussion of selectivity within some of these binding sites then follows.

Structure	λ step	Total sim. time (ns)
Bulk water	0.05	$40.0(Na^+)$, $8.0(Li^+, Rb^+, Cs^+)$
Model systems	0.05	40.0 (S,SS), 8.0(SB)
$k \neq 0$ model systems	variable	136
Na^+ channel Model	0.05	40.0
Glt_{Ph}	0.025 & 0.05	9.6
DNA quadruplex	0.05	4.0
ARK	0.1	2.0
Valinomycin	0.05	4.0
18-crown-6	0.05	4.0

Table 7: Parameters used in alchemical free energy perturbation simulations of model systems and biological molecules. Simulations include solvation boxes, lipid bilayers etc. S, SS and SB indicate sphere, sphere in a sphere and sphere in a box model ligand systems respectively.

The Na^+ channel selectivity filter model utilised the DEKA (aspartic acid, glutamic acid, lysine, alanine) motif in order to produce a near planar
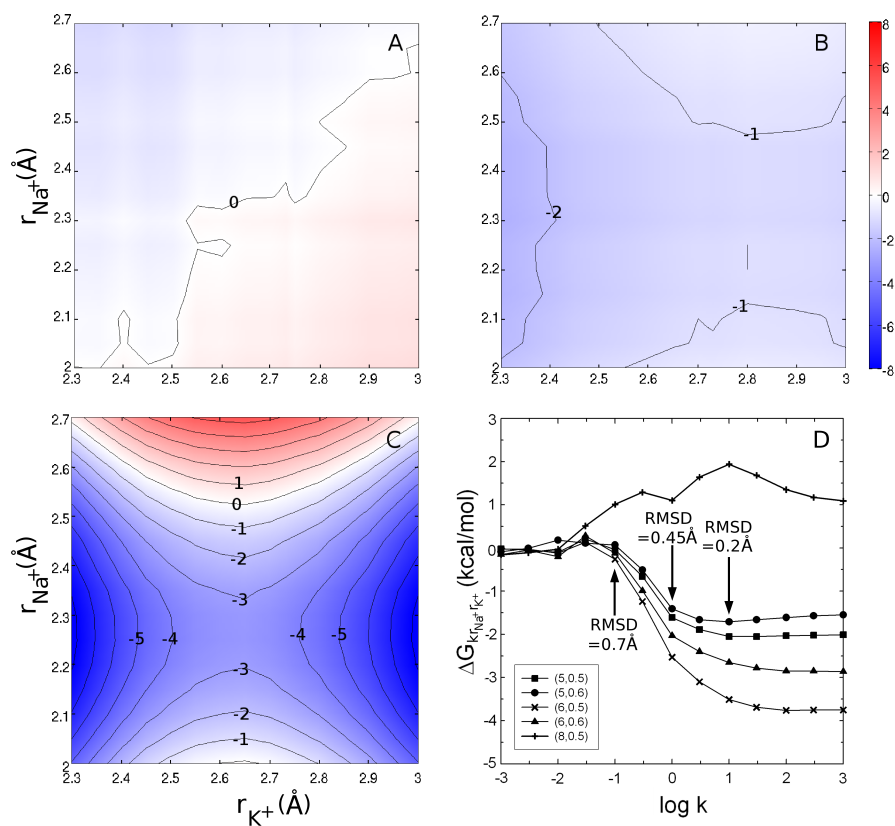
Figure 10: Influence of cavity size and ligand thermal fluctuations on ion selectivity with (A) $k = 0.03$ kcal/mol/Å^2, (B) $k = 0.3$ kcal/mol/Å^2 and (C) $k = 3.0$ kcal/mol/Å^2. Contour lines represent 1 kcal/mol differences in ΔG. (D) The effect of decreasing the ligand RMSD on selectivity for 5 different systems with different values of partial charge and ligand number. Cases with 5 or 6 ligands correspond to binding sites in the transporters, while that with 8 to KcsA. Arrows indicate the RMSD at specific k values for the $(n, q) = (6, 0.5)$ system.

Structure	$\Delta G_{K^+ \rightarrow Na^+}$	$\Delta G_{Na^+ \rightarrow K^+}$
Bulk water	-21.05	21.07
Na^+ channel Model	-25.8	27.0
Glt$_{Ph}$ Na1	-22.2	22.4
Glt$_{Ph}$ Na2	-20.3	23.1
DNA quadruplex	-15.7	18.4
ARK	-19.9	19.6
Valinomycin	-13.8	13.8
Nonactin	-20.9	21.0
18-crown-6	-18.3	18.5

Table 8: Forward and reverse ΔG values for each of the simulated systems. All values are in kcal/mol.

structure of these four amino acids. An approximately 4.4×4.4 Å rectangular gap was left to simulate the pore (32), the boundaries of which were determined by the inward facing side chain groups. Harmonic constraints of 2.2 kcal/mol/Å^2 was placed on the backbone carbon and nitrogen atoms to yield realistic RMSD fluctuations of the atoms. Each amino acid was N and C terminated.

The aspartate transporter (Glt$_{Ph}$), PDB code 2NWX (33), was placed in a POPC lipid bilayer which was solvated on both sides by an approximately 25 Å deep 120 mM NaCl solution. The transported aspartate was in zwitterionic form (34). The morphing Na^+ and K^+ were held fixed during the simulations. The system was equilibrated for 2 ns prior to FEP calculations. 24 λ windows of 400 ps each were simulated with two window sizes; 0.025 when $0 < \lambda < 0.1, 0.9 < \lambda < 1.0$ and 0.05 elsewhere. The system utilised periodic boundary conditions. There were 144255 atoms in total. The forward and reverse morph differ by 2.8 kcal/mol. As a consequence, the $Na^+ \rightarrow K^+$ morph was simulated an additional two times, and the average of these three simulations was taken.

Valinomycin, Cambridge structural database (CSD) code VALINK (35), was placed in a 30×30×30 Å periodic ethanol box and equilibrated for 4 nanoseconds. The Na^+ and K^+ ion was held in a fixed position at the centre of the box around which the valinomycin was placed. There were 9170 atoms in total.

Nonactin, CSD code NONACS (36), was placed in a 45×45×45 Å periodic

ethanol box, and the Na^+ and K^+ ions were held fixed in the centre as above. There were 9119 atoms in total.

18-crown-6, CSD code KTHOXD (37), was placed in a $30{\times}30{\times}24$ Å periodic water box with a Na^+ and K^+ atom fixed at the centre of the crown ether.

The G-quadruplex DNA structure, PDB code 1L1H (38), was solvated in a $55 \times 55 \times 55$ Å box of 300mM KCl solution and equilibrated for 15 ns prior to commencement of FEP calculations. Periodic boundary conditions were used. There were 16987 atoms in total.

The enzyme aminoimidazole riboside kinase (ARK), PDB code 1TYY (39), was solvated in an $80{\times}70{\times}117$ Å box of 120mM NaCl solution. Periodic boundary conditions were used. There were 59629 atoms in total.

All simulations were conducted using NAMD (40) with the CHARMM27 (41) force field, unless otherwise noted, at 310 K and 1 atm with 1 fs timesteps.

Valinomycin

Valinomycin is an interesting case. In a previous study, it was demonstrated that the predominant contributor toward K^+ selectivity comes from cavity size effects (42). In our initial studies conducted in vacuum, the Na^+ ion bounces around in the valinomycin cavity, unable to find a favourable Na^+-ligand distance simultaneously for all ligands, whilst K^+ is able to do so giving it a 12.1 kcal/mol selectivity over Na^+ , which is in good agreement with density functional calculations (12.3 kcal/mol) (42). The rigidity of the valinomycin is enforced by intermolecular hydrogen bonding, which maintains its ring like structure (Fig. 11 A & B). In vacuum, therefore, the cavity size of valinomycin appears to give the largest contribution to its K^+ selectivity.

Once valinomycin is placed in a solvent, however, additional factors come into play. While the K^+/valinomycin complex in ethanol behaves similarly to its vacuum counterpart, when Na^+ is present inside the cavity, the valinomycin distorts significantly from a ring into a oval shape (Fig. 11 C). Although the coordination number of 6 is maintained by Na^+ between the two environments, it is not bound to the same ligands. As a result of attempting to optimise the coordination distance, Na^+ coordinates to only 4 of the original 6 oxygens where one of the additional ligands is sourced from a previously hydrogen bonded oxygen and another from an ethanol oxygen

(Fig. 11 D). The breaking of this hydrogen bond allows the valinomycin to distort. The remaining two oxygens that participated in K^+ coordination hydrogen bond to ethanol when Na^+ is bound. The ability of Na^+ to gain a more optimal coordination number reduces the selectivity of the molecule, leading to a K^+ selectivity of 7.2 kcal/mol. This also indicates that coordination number restriction cannot underlie this selectivity. As the cavity size has altered to favourably coordinate both K^+ and Na^+, our analysis attributes the selectivity to the intrinsic dipole moment of the coordinating ligands. The change in selectivity between gas and ethanol, however, is not as large as may be suspected from our selectivity maps due to the added energy cost of breaking a hydrogen bond when coordinating Na^+. This energy cost represents a deformation energy intrinsic to this particular molecule that cannot be captured in our model systems. While this energy would be small in large proteins where the coordinating ligands are not directly attached to one another, it may be more significant in small cyclic molecules. This deformation energy could be considered part of the cavity size effect as it represents the cost incurred in adapting the cavity to the size of each ion, but is not included in our definition. Comparing our predicted and simulated selectivities in valinomycin suggests that the deformation energy may be as great as 4.2 kcal/mol. This equates to 60% of the total selectivity coming from cavity size molecular deformation, leaving 25% and 15% contribution from coordination number restriction, χ_n, and dipole moments, χ_q, respectively. Using both methods, we find the size and importance of this deformation energy is consistent with the findings of Varma and Rempe (42).

18-Crown-6

In 18-crown-6, shown in Fig. 12, the K^+ ion coordinates to the six oxygen molecules in the crown as well as coordinating to two water molecules axially. The Na^+ ion coordinates to only four of the six crown oxygens, plus to two axial water molecules. Thus, both can optimise their coordination numbers. The flexibility of the cavity size means that the overall selectivity of the molecule is attributed to the intrinsic dipole moment of the ligands. But, as with valinomycin, in the presence of Na^+ the crown ether deforms so that the two uncoordinated crown oxygens may coordinate with the bulk water. This again creates a small energy cost not captured in our maps.
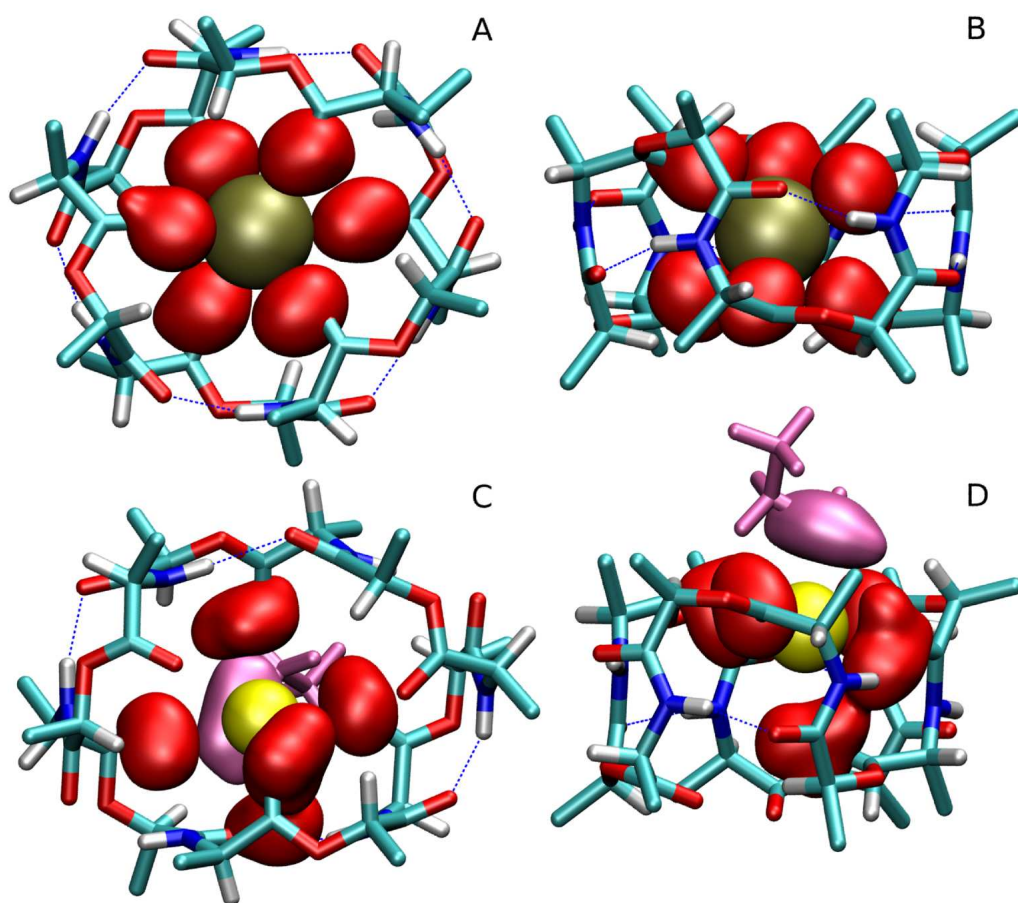
Figure 11: Structures of K^+ and Na^+ complexed with valinomycin in an ethanol box. 'Side chain' atoms in valinomycin have been removed for clarity. K^+ is brown, Na^+ yellow, oxygen red, carbon cyan, nitrogen blue, hydrogen white and ethanol is magenta. The red and magenta surfaces show the regions of space visited by the mobile coordinating oxygens. Hydrogen bonding is denoted by dashed blue lines. (A) Top view of K^+/valinomycin complex. (B) Side view of K^+/valinomycin complex. (C) Top view of Na^+/valinomycin complex showing the distorted shape of the molecule and the participation of ethanol in ion coordination. (D) Side view of Na^+/valinomycin demonstrating the disruption of the hydrogen bonding within valinomycin and the shift of Na^+ to one edge of one of the valinomycin ring.
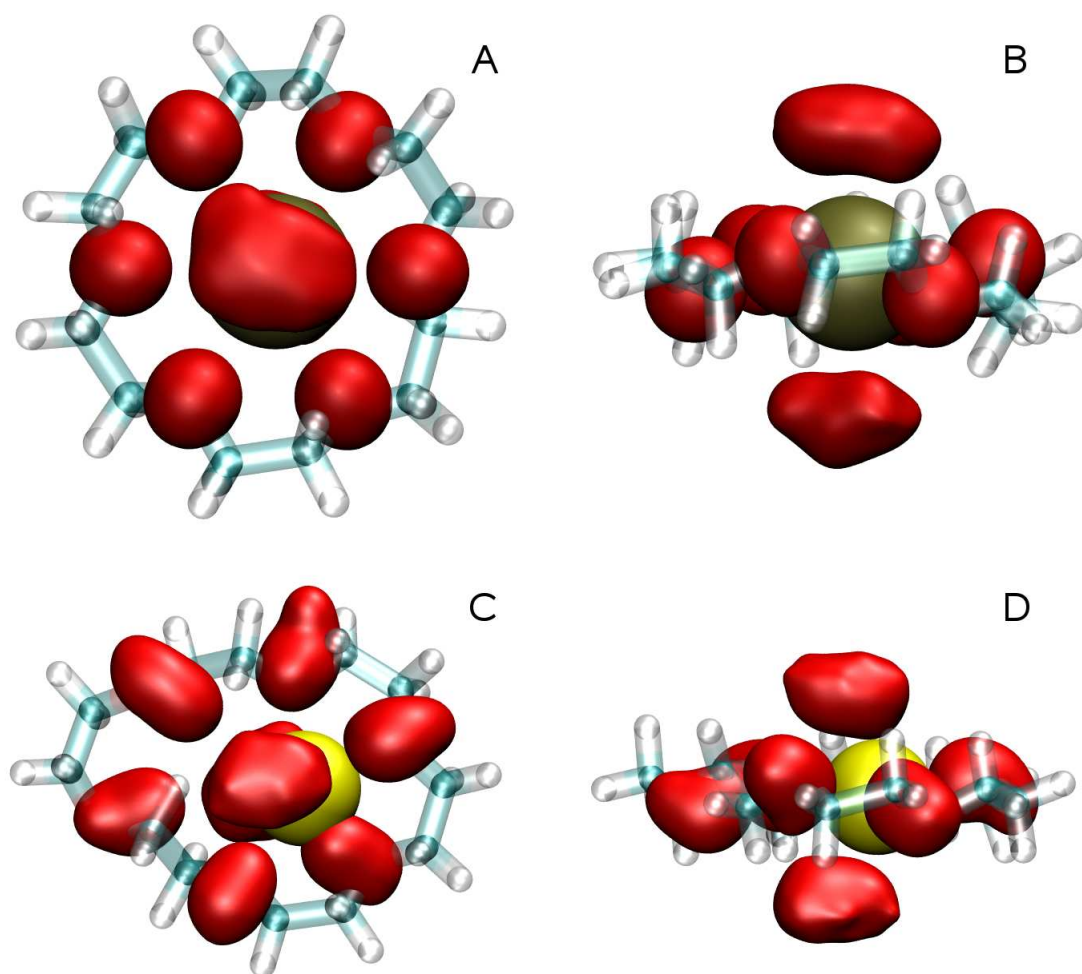
19

Figure 12: Structures of 18-crown-6 complexed with K^+ or Na^+ in water. Solid red surfaces indicate the regions of space visited by the coordinating oxygen atoms of the crown or water molecules. K^+ is brown and Na^+ yellow. Transparent atoms represent carbon (cyan), hydrogen (white) and oxygen (red). (A) Top view and (B) side view of K^+/18c6 complex. (C) Top view and (D) side view of Na^+/18c6 complex. Note the deformation of the crown structure in the presence of Na^+ compared with that obtained with K^+. Not all all oxygens coordinate Na^+ simultaneously, as evidenced by the offset position of the Na^+ and the elongated region of space occupied by the oxygen atoms as they approach and recede from the ion.

ARK, LeuT and Glt$_{Ph}$

Contributions to ion selectivity from restricted ligand mobility were most notable in the two amino acid transporters in which the ligands appear constrained in their movement. The RMSD of the coordinating ligands in Glt$_{Ph}$ with Na$^+$ bound was 0.30 and 0.30 Å for site 1 and 2 and with K$^+$ was 0.52 and 0.35 Å. The same RMSD in LeuT was 0.39 and 0.43 Å when Na$^+$ was bound to site 1 and site 2 (43), while the K$^+$ bound values are not known. These low RMSD values may be a consequence of the coordinating ligands being part of an α helix and thus held in place through networks of hydrogen bonding.

In contrast to these situations, the ligands forming the binding site of the enzyme ARK are primarily associated with protein loops as shown in Fig. 13. These tend to be much more flexible than α helices, so we would expect that this could produce a more flexible environment in which the binding cavity size and restricted ligand mobility would have a smaller impact on the overall selectivity. This is exactly what we see. The average ion-ligand distance in ARK changes from 2.3 Å for Na$^+$ to 2.7 Å for K$^+$ indicating that restrictions on cavity size do not contribute to ion selectivity in this case, and the RMSD of the coordinating atoms is 0.55-0.6 Å.
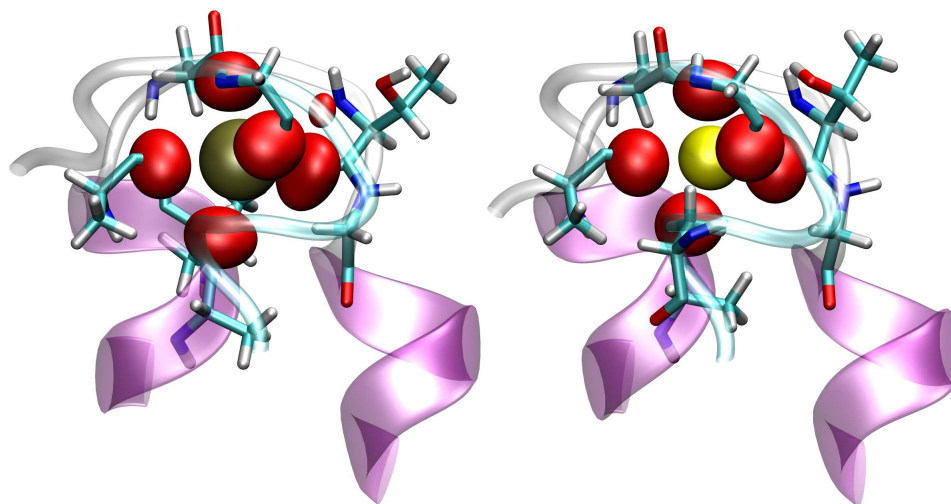
Figure 13: Structures of the ion binding site in ARK in complex with (A) K^+ and (B) Na^+. Residues directly participating in ion coordination are shown in an all atom representation while the surrounding protein is shown by the cartoon. The regions of space visited by the coordinating oxygen atoms are shown by red surfaces. Note that one oxygen atom is hidden behind the ion in each picture. The small red surface near in the top right in (A) represents the occasional presence of a water molecule coordinating K^+.

References

1. Jorgensen, W., and J. Tirado-Rives, 1988. The OPLS potential function for protein, energy minimizations for crystals of cyclic peptides and crambin. *J. Am. Chem. Soc.* 110:1657–1666.

2. Jensen, K., and W. Jorgensen, 2006. Halide, ammonium, and alkali metal ion parameters for modeling aqueous solutions. *J. Chem. Theory Comput.* 2:1499–1509.

3. Yellen, G., 1984. Ionic permeation and blockade in Ca^{2+} activated K^+ channels of bovine chromaffin cells. *J. Gen. Physiol* 84:157–186.

4. Heginbotham, L., and R. MacKinnon, 1993. Conduction properties of the cloned Shaker channel. *Biophys. J.* 65:2089–2096.

5. LeMasurier, M., L. Heginbotham, and C. Miller, 2001. KscA: it's an ion channel. *J. Gen. Physiol* 118:303–314.

6. Nimigean, C. M., and C. Miller, 2002. Na^+ block and permeation in K^+ channel of known structure. *J. Gen. Physiol* 120:323–325.

7. Pranata, J., and W. L. Jorgensen, 1991. Monte Carlo Simulations Yield Absolute Free Energies of Binding for Guanine-Cytosine and Adenine-Uracil Base Pairs in Chloroform. *Tetrahedron* 47:2491–2501.

8. Gilson, M. K., J. A. Given, B. L. Bush, and J. A. McCammon, 1997. The statistical-thermodynamic basis for computation of binding affinities: a critical review. *Biophys. J.* 72:1047–1069.

9. Kasterholz, M. A., and P. H. Hünenbuger, 2006. Computation of methodology-independent ionic solvation free energies from molecular simulations. II. The hydration free energy of the sodium cation. *J. Chem. Phys.* 124:224501.

10. Kameda, Y., S. Suzuki, H. Ebata, T. Usuki, and O. Uemura, 1997. The short-range structure around Li^+ in highly concentrated aqueous LiBr. *Bull. Chem. Soc. Jpn.* 70:47–53.

11. Kameda, Y., K. Sugawara, T. Usuki, and O. Uemura, 1998. Hydration structure of Na^+ in concentrated aqueous solutions. *Bull. Chem. Soc. Jpn.* 71:2769–2776.

12. Smirnov, P., and V. Trostin, 2007. Structures of the nearest surroundings of the K^+, Rb^+ and Cs^+ ion in aqueous solutions of their salts. *Russ. J. Gen. Chem.* 77:2101–2107.

13. Noskov, S., S. Bernèche, and B. Roux, 2004. Control of ion selectivity in potassium channels by electrostatic and dynamic properties of carbonyl ligands. *Nature* 431:830–834.

14. Noskov, S., and B. Roux, 2007. Importance of hydration and dynamics on the selectivity on the KcsA and NaK channels. *J. Gen. Physiol.* 129:135–143.

15. Noskov, S., and B. Roux, 2008. Control of ion selectivity in LeuT: two Na^+ binding sites with two different mechanisms. *J. Mol. Biol* 377:804–818.

16. Beglov, D., and B. Roux, 1994. Finite representation of an infinite bulk system: solvent boundary potential for computer simulations. *J. Chem. Phys.* 100:9050–9063.

17. Schwenk, C., T. Hofer, and B. Rode, 2004. "Structure breaking" effect of hydrated Cs^+. *J. Chem. Phys. A* 108:1509–1514.

18. Varma, S., and S. Rempe, 2006. Coordination numbers of alkali metal ions in aqueous solutions. *Biophys. Chem.* 124:192–199.

19. Ansell, S., A. Barnes, P. Mason, G. Neilson, and S. Ramos, 2006. X-ray and neutron scattering studies of the hydration structure of alkali ion in concentrated aqueous solution. *Biophys. Chem.* 124:171–179.

20. Lee, S., and J. Rasaiah, 1996. Molecular dynamics simulations of ion mobility. 2. Alkali metal and halide ions using the SPC/E model for water at 25 °C. *J. Phys. Chem.* 100:1420–1425.

21. Azam, S., T. Hofer, B. Randolf, and B. Rode, 2009. Hydration of sodium(I) and potassium (I) revisited: A comparitive QM/MM and QMCF MD simulation study of weakly hydrated ions. *J. Phys. Chem.* 113:1827–1834.

22. Fulton, J., D. Pfund, S. Wallen, M. Newville, E. Stern, and Y. Ma, 1996. Rubdium ion hydration in ambient and supercritical water. *J. Chem. Phys.* 105:2161–2166.

23. Ramos, S., A. Barnes, G. Neilson, and M. Capitan, 2000. Anomalous X-ray diffraction studies of hydration effects in concentrated aqueous electrolyte solutions. *Chem. Phys.* 258:171–180.

24. Hofer, T., B. Randolf, and B. Rode, 2005. Stucture-breaking effects of solvated RbI in dilute aqueous solution - an ab initio QM/MM MD approach. *J. Comput. Chem.* 26:949–956.

25. Bertagnolli, H., T. Ertel, M. Hoffmann, and R. Frahm, 1991. EX-AFS studies of aqueous solutions of rubidium bromide. *Berich. Bunsen. Gesell.* 95:704–709.

26. Ohtomo, N., and K. Arakawa, 1979. Neutron diffraction study of aqueous ionic solutions I. Aqueous solutions of Lithium Chloride and Caesium Chloride. *B. Chem. Soc. Jpn.* 52:2755–2759.

27. Novikov, A., M. Rodnikova, V. Savostin, and O. Sobolev, 1999. The study of hydration effects in aqueous solutions of LiCl and CsCl by inelastic neutron scattering. *J. Mol. Liq.* 82:83–104.

28. Ramos, S., G. Neilson, A. Barnes, and P. Buchanan, 2005. An anomalous x-ray diffraction study of the hydration structures of Cs^+ and I^- in concentrated solutions. *J. Chem. Phys.* 123:214501 – 214501–10.

29. Fowler, P., K. Tai, and M. Sansom, 2008. The selectivity of K^+ ion channels: Testing the hypotheses. *Biophys. J.* 95:5062–5072.

30. Bostick, D., and C. Brooks, 2007. Selectivity in K^+ channels is due to topological control of the permeant ion's coordinated state. *PNAS* 104:9260–9265.

31. Thomas, M., D. Jayatilaka, and B. Corry, 2007. The predominant role of coordination number in potassium channel selectivity. *Biophys. J.* 93:2635–2643.

32. Vora, T., B. Corry, and S. Chung, 2004. A model of sodium channels. *BBA* 1668:106–116.

33. Boudker, O., R. Ryan, D. Yernool, K. Shimamoto, and E. Gouaux, 2007. Coupling substrate and ion binding to extracellular gate of a sodium-dependent aspartate transporter. *Nature* 445:387–393.

34. Wingrove, T., and G. Kimmich, 1988. Low-affinity intestinal L-aspartate transport with 2:1 coupling stoichiometry for Na^+/Asp. *Am. J. Physiol Cell Physiology* 255:C737–C744.

35. Neupert-Laves, K., and M. Dobler, 1975. The crystal structure of a K^+ complex of Valinomycin. *Helv. Chim. Acta* 58:432–442.

36. Dobler, M., and R. Phizackerley, 1975. The crystal structure of the NaNCS complex of nonactin. *Helv. Chim. Acta* 57:664–674.

37. Seiler, P., M. Dobler, and J. Dunitz, 1974. Potassium thiocyanate complex of 1,4,7,10,13,16-Hexaoxacyclooctadecane. *Acta Cryst. Sect. B.* 30:2744–2745.

38. Haider, S., G. Parkinson, and S. Neidle, 2003. Structure of a G-quadruplex-ligand complex. *J. Mol. Biol.* 326:117–125.

39. Zhang, Y., M. Dougherty, D. Downs, and S. Ealick, 2004. Crystal structure of an aminoimidazole riboside kinase from *Salmonella enterica* Implications for the evolution of the ribokinase superfamily. *Structure* 12:1809–1821.

40. Phillips, J. C., R. Braun, W. Wang, J. Gumbart, E. Tajkhorshid, E. Villa, C. Chipot, R. D. Skeel, L. Kale, and K. Schulten, 2005. Scalable molecular dynamics with NAMD. *J. Comp. Chem.* 26:1781–1802.

41. MacKerell Jr., A. D., D. Bashford, M. Bellott, R. L. Dunbrack Jr., J. D. Evanseck, M. J. Field, S. Fischer, J. Gao, H. Guo, S. Ha, D. Joseph-McCarthy, L. Kuchnir, K. Kuczera, F. T. K. Lau, C. Mattos, S. Michnick, T. Ngo, D. T. Nguyen, B. Prodhom, W. E. R. III, B. Roux, M. Schlenkrich, J. C. Smith, R. Stote, J. Straub, M. Watanabe, J. Wiorkiewicz-Kuczera, D. Yin, and M. Karplus, 1998. All-Atom Empirical Potential for Molecular Modeling and Dynamics Studies of Proteins. *J. Phys. Chem. B.* 102:3586–3616.

42. Varma, S., D. Sabo, and S. Rempe, 2008. K^+ and Na^+ selectivity in K channels and valinomycin: over-coordination versus cavity-size constraints. *J. Mol. Biol.* 376:13–22.

43. Celik, L., B. Schiøtt, and E. Tajkhorshid, 2008. Substrate binding and formation of an occluded state in the leucine transporter. *Biophys. J.* 94:1600–1612.